where $\xi = \varepsilon\sigma T^3 D/k_o$. For ξ less than about six, this is closely approximated by

$$\frac{k_o T}{\delta} - \dot{m}(H_s - H_\infty) = \varepsilon\sigma T^4 \frac{\delta}{D} e^{-2\xi/7}$$

where the right-hand side is the total side radiation flux, $\dot{q}_{rs}$. Solving for δ and substituting the result in the right-hand side gives

$$\dot{q}_{rs} = \left[\left(\frac{\dot{q}_{ko}}{2}\right)^2 + \dot{q}_d \dot{q}_r \exp\left(-\frac{2\dot{q}_r}{7\dot{q}_d}\right)\right]^{1/2} - \frac{\dot{q}_{ko}}{2}$$

where $\dot{q}_{ko} = \dot{m}(H_s - H_\infty)$, $\dot{q}_d = k_o T/D$, and $\dot{q}_r = \varepsilon\sigma T^4$.

References

[1] Lees, L., "Convective Heat Transfer with Mass Addition and Chemical Reactions," *Recent Advances in Heat and Mass Transfer*, edited by J. P. Hartnett, McGraw-Hill, New York, 1961.

[2] Hearne, L. F., Gallagher, L. W., and Woodruff, L. W., "Surface Oxidation with Streamwise Variation of Wall Reactivity," *AIAA Progress in Astronautics and Aeronautics: Thermal Design Principles of Spacecraft and Entry Bodies*, Vol. 21, edited by J. T. Bevans, Academic Press, New York, 1969, pp. 225–248.

[3] Dolton, T. A., Maurer, R. E., and Goldstein, H. E., "Thermodynamic Performance of Carbon in Hyperthermal Environments," *AIAA Progress in Astronautics and Aeronautics: Thermal Design Principles of Spacecraft and Entry Bodies*, edited by J. T. Bevans, Academic Press, New York, 1969, pp. 169–201.

[4] Kratsch, K. M., Martinez, M. R., Clayton, F. I., Greene, R. B., and Wuerer, J. E., "Graphite Ablation in High-Pressure Environments," AIAA Paper 68-1153, Williamsburg, Va., Dec. 1968.

[5] Moody, H. L., Sherman, M. M., Dunn, S. S., and Haddock, R. L., "The Development and Application of a Tungsten Ablation Model for Reentry Environments," PDA TR 1013-00-05, Jan. 1974, Prototype Development Associates, Inc., Costa Mesa, Calif.

[6] Ziering, M. B. and DiCristina, V., "Thermomechanical Erosion of Ablative Plastic Composites," AIAA Paper 72-299, San Antonio, Texas, April 1972.

[7] *JANAF Thermochemical Tables*, Dow Chemical Company, Midland, Mich., incl. Supplement No. 41, June 1974.

[8] Hartnett, J. P., "Mass Transfer Cooling," *Handbook of Heat Transfer*, edited by W. M. Rohsenow and J. P. Hartnett, McGraw-Hill, New York, 1973.

[9] Rubesin, M. W. and Inouye, M., "Forced Convection, External Flows," *Handbook of Heat Transfer*, edited by W. M. Rohsenow and J. P. Hartnett, McGraw-Hill, New York, 1973.

[10] Schick, H. L., *Thermodynamics of Certain Refractory Compounds*, Vol. II, Academic Press, New York, 1966.

[11] Hansen, M., *Constitution of Binary Alloys*, 2nd ed., McGraw-Hill, New York, 1958.

[12] Elliott, R. P., *Constitution of Binary Alloys, First Supplement*, McGraw-Hill, New York, 1965.

[13] "Avco Hyperthermal Simulation Capabilities," Rept. AVSD-0457-70-CA, Sept. 1970, Avco Systems Division, Wilmington, Mass.

MAY 1975 AIAA JOURNAL VOL. 13, NO. 5

Vectored Injection into Laminar Boundary Layers with Heat Transfer

G. R. INGER* AND T. F. SWEAN†
Virginia Polytechnic Institute and State University, Blacksburg, Va.

A basic theoretical investigation of self-similar isobaric laminar two-dimensional or axisymmetric boundary-layer flows is presented for a wide range of normal and tangential surface mass transfer velocities ("vectored" injection and suction) in the presence of heat transfer. Vanishingly-small skin friction conditions pertaining to incipient separation are included. A new set of double-valued solutions pertaining to the case of small-to-moderate upstream vectoring is identified and studied. Also, the frictional heating associated with vectoring is shown to have a significant effect on the heat transfer and recovery factor for high-speed flows. Detailed results are presented for skin friction, velocity and enthalpy profiles, and momentum, and displacement thickness integral properties.

Nomenclature

C_p = constant pressure specific heat
f_w = normal injection parameter
f'_w = tangential injection parameter
g_w = surface total enthalpy ratio
h, H = static and total enthalpy, respectively ($H = h + u^2/2$)
$I_0 = \int_0^\infty (g - f')\, d\eta$
$I_1 = \int_0^\infty (g - f'^2)\, d\eta$
$I_2 = \int_0^\infty f'(1 - f')\, d\eta$
M = Mach number
Pr = Prandtl number
$\dot{q}_w$ = surface heat transfer rate
r_B = body radius
Re_x = Reynolds number, $\rho_e u_e x/\mu_e$
T = static temperature
u, v = velocity components in x, y coordinate directions
x, y = streamwise and normal physical coordinates
Z = recovery factor parameter (Eq. 12)
γ = ratio of specific heats
δ = boundary-layer thickness
δ^* = boundary-layer displacement thickness
ε = 0, 1 for $2-D$ and axisymetric flow, respectively

Presented as Paper 74-676 at the AIAA/ASME 1974 Thermophysics and Heat Transfer Conference, Boston, Massachusetts, July 15–17, 1974; submitted August 19, 1974; revision received October 16, 1974. Research was supported by the National Science Foundation under Grant NSF-6K20379 and by the Air Force Office of Scientific Research under Grant 72-2173.

Index category: Boundary Layers and Convective Heat Transfer—Laminar.

* Professor, Department of Aerospace and Ocean Engineering. Associate Fellow AIAA.

† Graduate Research Assistant, Department of Aerospace and Ocean Engineering.

η $= \left(u_e r_B^{\varepsilon} \int_o^y \rho\, dy\right) \Big/ (2\xi)^{1/2}$
θ^* = momentum thickness
μ = viscosity
ξ $= \int_o^x \rho_w \mu_w u_e r_B^{2\varepsilon}\, dx$
ρ = flow density
τ_w = shear stress at surface

Subscripts

e = edge of boundary layer
w = flow conditions at wall surface
aw = adiabatic wall flow conditions

Superscripts

$(\,)' = \partial/\partial\eta$

I. Introduction

THE theoretical study of surface mass transfer effects involving both normal and tangential components ("vectored" suction or injection) finds application in a number of important boundary-layer flow problems, such as a) film and transpiration cooling of rocket engines, turbine blades, and surfaces of high-speed aerodynamic bodies, b) mass transfer and mixing processes in pollution problems, c) flow in the blown-off shear layer of radiatively heated massively-ablating planetary re-entry bodies, d) boundary-layer flows past permeable or moving belt-surfaces with mass transfer found in industrial manufacturing devices and processes, e) the effect of high-altitude (low-density) surface slip and temperature jump phenomena on mass transfer and heat transfer in rarefied flows, and f) use of suction and blowing for boundary-layer control on aerodynamic vehicles. There are relatively few analyses available which consider this general vectored mass transfer problem, however, and these are limited to a rather small range of the possible normal and tangential velocities for the case of injection (blowing) into adiabatic flows.[1-3] The purpose of the present paper is to describe the results of a comprehensive systematic basic investigation of vectoring over a wide range of interesting physical conditions for suction as well as injection, including the effects of heat transfer.

To focus attention on the effects uniquely related to vectoring, we confine our attention in this first phase of investigation to homogeneous suction or blowing into isobaric ($\partial pe/\partial x = 0$) self-similar laminar boundary-layer flows. The present work thus extends a previous investigation[7] to nonadiabatic flows and the case of suction as well as injection. The resulting solutions yield valuable insight and a first approximation (via the well-established local similarity approximation[4,5]) to the influence of vectored suction and injection on various physical properties of interest in the aforementioned applications, such as boundary-layer velocity and temperature profiles, skin friction, heat transfer, recovery factor, and displacement thickness. Moreover, our solutions are useful elements in devising approximate nonsimilar solution techniques such as modern integral methods.[6] Of more fundamental interest, we show the existence of a new previously-overlooked "branch" of solutions pertaining to certain ranges of upstream mass transfer vectoring. Also, it is shown that the frictional heating associated with vectoring contributes a heretofore-ignored effect which can be very significant on the recovery temperature properties of the flow.

II. Formulation of the Analysis

We consider steady laminar flow past a two-dimensional or axisymmetric surface at sufficiently high Reynolds number to justify boundary-layer approximations. The influence of longitudinal surface curvature and the so-called transverse curvature effect associated with slender axisymmetric bodies are both neglected. Longitudinal pressure gradients are also assumed to be negligible. Fluid or a perfect gas of the same type as the mainstream can be either injected or withdrawn through the surface (e.g., the surface may be porous); the two are assumed not to react, however. The density-viscosity product $\rho\mu$ is assumed constant across the boundary layer, as is the Prandtl number Pr (nonunity values of the latter are considered).

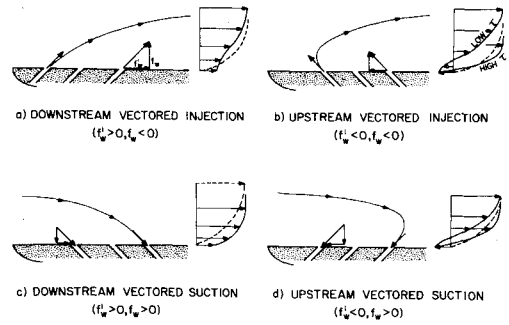

Fig. 1 Schematic illustration of various vectored mass transfer cases.

Introducing a stream function $\psi = (2\xi)^{1/2} f(\xi, \eta)$ in terms of the Levy-Lees similarity variables η, ξ defined in the nomenclature, the aforementioned assumptions lead to the following well-known momentum and energy equations governing self-similar flow:

$$f''' + ff'' = 0 \tag{1}$$

$$g'' + Prfg' + (Pr-1)(u_e^2/2H_e)(f'^2)' = 0 \tag{2}$$

where $f'(\eta) = u/u_e$ and $g = H/H_e$. The corresponding outer boundary conditions are the usual ones

$$f'(\infty) = g(\infty) = 1 \tag{3}$$

while those at the surface with vectored mass transfer and any given wall temperature are

$$f'(0) \equiv f'_w = u_w/u_e = \text{given} \tag{4a}$$

$$f(0) \equiv f_w = \frac{-\rho_w v_w (2\xi)^{1/2} r_B^{\varepsilon}}{\partial\xi/\partial x} = \text{given} \tag{4b}$$

$$g(0) \equiv g_w = \frac{h_w}{H_e} + \left(\frac{u_e^2}{2H_e}\right) f_w'^2 \quad (h_w \text{ given}) \tag{4c}$$

where f_w and f'_w represent the normal and tangential velocities at the surface, respectively, being positive constants for suction and downstream vectoring while negative constants for blowing and upstream vectoring, respectively. A schematic illustration of the four different physical cases involved which we shall consider is given in Fig. 1. Their physical realization and utility will be discussed later.

In terms of the parameters f_w and f'_w, the actual resultant injection velocity and its vector angle θ_B with respect to the wall are given by $(u_w/u_e)^2 + (v_w/u_e)^2 = (f'_w)^2 + T_w^2 f_w^2 (\partial\xi/\partial x)/2Re_x \cdot (\xi/x) T_e^2$ and $\tan\theta_B = -T_w f_w / T_e f'_w [2Re_x(\xi/x)/\partial x/\partial\xi]^{1/2}$, respectively.‡ As indicated by the example shown in Table 1, the addition of just a moderate amount of tangential injection in a high Reynolds number flow reduces the angle θ_B to very small values even in the presence of large normal mass transfer, especially on a cold wall ($T_w \ll T_e$).

Table 1 Tangential velocity effect on injection angle ($Re_x = 5 \times 10^3$, $f_w = -1$)

	θ_B, degrees	
f'_w	$T_w = T_e$	$T_w = 0.10 T_e$
0.00	90.0	90.0
0.01	45.0	5.7
0.10	5.7	0.6
1.00	0.6	0.06

‡ The quantity $(\partial\xi/\partial x)/(\xi/x)$, which appears frequently, has the value $(2\varepsilon + 1)$ for the isobaric case considered in this paper.

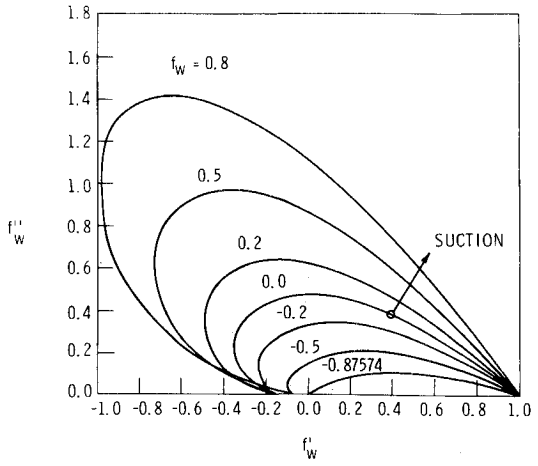

Fig. 2 Mass transfer vectoring effect on wall shear parameter.

Once this boundary value problem is solved, the important gross physical properties of the flow can be found from the following relationships:

Skin Friction

$$\frac{\tau_w\left[2\left(\frac{\xi/x}{\partial\xi/\partial x}\right)Re_x\right]^{1/2}}{\rho_e u_e^2} = f''(0) \equiv f''_w \tag{5}$$

Heat Transfer

$$\frac{\dot{q}_w Pr\left[2\left(\frac{\xi/x}{\partial\xi/\partial x}\right)Re_x\right]^{1/2}}{\rho_e u_e H_e} = (h/H_e)'_w + Pr(u_e^2/2H_e)(2f'_w f''_w) \tag{6a}$$

$$= g'_w - \frac{u_e^2}{2H_e}(1-Pr)(2f'_w f''_w) \tag{6b}$$

Displacement Thickness

$$\frac{\delta^*}{x}\left(\frac{Re_x\,\partial\xi/\partial x}{2\xi/x}\right)^{1/2} = \int_0^\infty (g-f')\,d\eta + \frac{u_e^2}{2h_e}\int_0^\infty (g-f'^2)\,d\eta$$

$$\equiv I_o + \frac{u_e^2}{2h_e} I_1 \tag{7}$$

Momentum Thickness

$$\frac{\theta^*}{x}\left(\frac{Re_x\,\partial\xi/\partial x}{2\xi/x}\right)^{1/2} = \int_0^\infty f'(1-f')\,d\eta \equiv I_2 \tag{8}$$

There is also the following Crocco-type energy equation solution for $Pr = 1$, valid for all values of both tangential and normal velocities at the surface:

$$g(\eta) = 1-(1-g_w)[1-f'(\eta)]/[1-f'_w] \tag{9}$$

where we note from Eq. (4c) that g_w itself depends on f'_w.

In carrying out the numerical solution of Eqs. (1–4), we confine our attention to cases with nonvanishing and positive wall shear ($f''_w > 0$); otherwise, solutions are studied over a much wider range of f_w and f'_w than considered previously including solutions for suction as well as blowing. In particular, the occurrence of a new branch of self-similar solutions pertaining to a limited range of upstream-injection velocities (first reported in Ref. 7) was extensively studied. The usual iterative technique of guess and shoot was found to be quite satisfactory in obtaining the numerical solutions: for each set of prescribed values of f_w, f'_w, g_w, $u_e^2/2H_e$, and Pr, trial values of f''_w and g'_w are selected and subsequently corrected until the outward integration of Eqs. (1) and (2) to some appropriately large value of η (15–30) satisfies the outer boundary conditions (3) to a specified degree of accuracy. This procedure was carried out on the IBM 370/155 computer using a variable integration step size to control the local truncation error. Convergence was considered achieved when $1-f'(\infty)$ and $f''(\infty)$ vanished to within six and ten decimal places, respectively. For the special case of

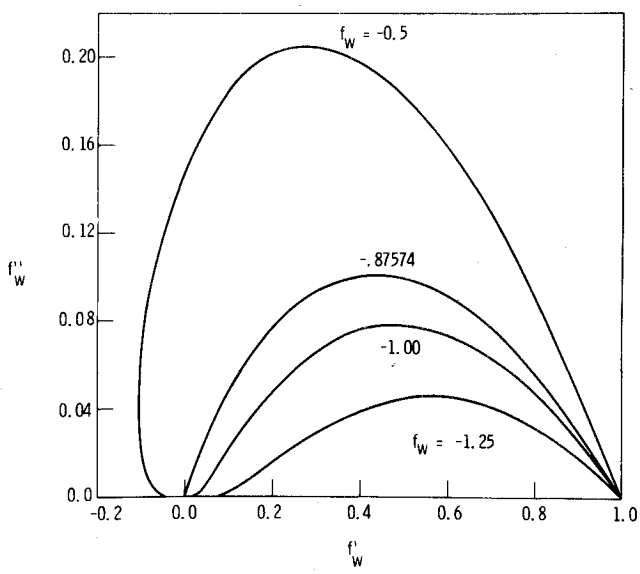

Fig. 3 Vectored injection effect on wall shear parameter.

$Pr = 1$, use was of course made of the solution Eq. (9). As a check, comparisons were made with Dewey and Gross's solutions[8] for zero pressure gradient. Our results agreed to within the four decimal places they tabulate for each case considered. Solutions of Eq. (1) were also compared with those previously obtained for adiabatic flow, five decimal place agreement being attained in all cases.

In the aforementioned manner, solutions were obtained for tangential and normal surface velocity conditions throughout the range $-1.25 \leqq f_w \leqq 0.8$ and $-0.96 \leqq f'_w \leqq 1.0$. Solutions were obtained for $Pr = 0.7$ and 1.0 and for wall enthalpies $0.0 \leqq g_w \leqq 1.0$. A complete summary of the results in the form of tabulated velocity and enthalpy profile solutions can be found in Ref. 9. The details of selected features of these results are illustrated and discussed in the following sections.

III. Discussion of Results

Velocity Field

In Figs. 2 and 3 the wall shear parameter f''_w is plotted as a function of the tangential surface velocity f'_w with the normal velocity at the surface f_w as a parameter. Figure 2 shows that when the normal injection velocity is less than the Emmons and Leigh[10] critical "blowoff" value ($f_w \geqq -0.87574$) one can obtain solutions over a limited range of upstream tangential injection velocities ($f'_w < 0$), these solutions being double-valued with high and low positive wall-shear values, respectively. On the other hand, solutions are also possible for "supercritical" blowing ($f_w < -0.87574$) with downstream vectoring, all of these being single valued (see Fig. 3). As shown in Fig. 2, small-to-

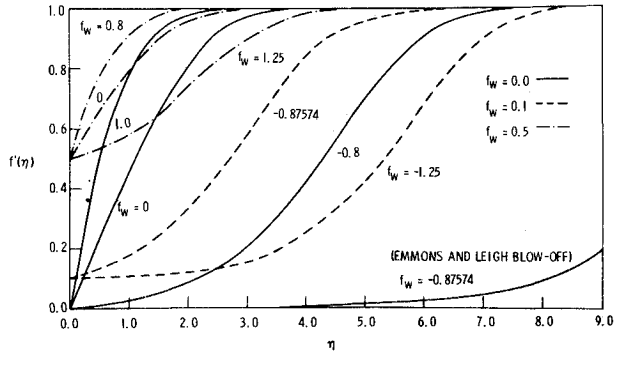

Fig. 4 Velocity profiles for downstream-vectored mass transfer.

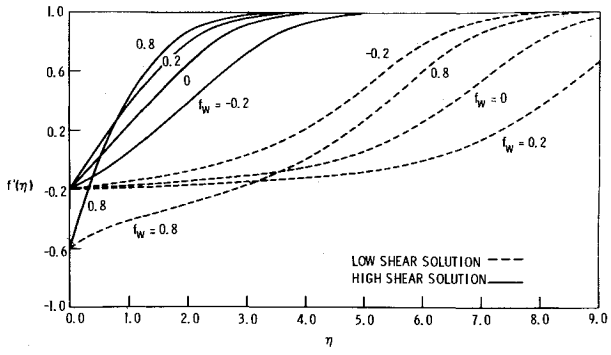

Fig. 5 Velocity profiles for upstream-vectored mass transfer.

moderate positive tangential velocities at the surface act like a favorable pressure gradient in increasing the wall shear in the presence of injection ($f_w \leqq 0$). However, with suction $f_w \geqq 0$ the reverse is true and the wall shear decreases with increasing f'_w. Figure 3 also shows that blowoff and separation ($f''_w = 0$) occur at much higher normal injection rates with downstream vectoring and that the amount of tangential blowing for maximum delay of separation (max f''_w points) increases as the normal injection rate increases.

The double-valued solutions pertaining to the second quadrant $f'_w < 0$ of Fig. 2 are obtained only for upstream-injection velocities below a certain maximum value that increases with the amount of suction (for example, the maxima corresponding to $f_w = 0$ and 0.8 are $f''_w = -0.354$ and -0.955, respectively). These solutions are analogous to the double-valued solution branch for adverse pressure gradients obtained by Cohen and Reshotko[11] in their well-known study on self-similar solutions to the boundary-layer equations. The existence of and distinction between the present pair of solutions can be physically explained

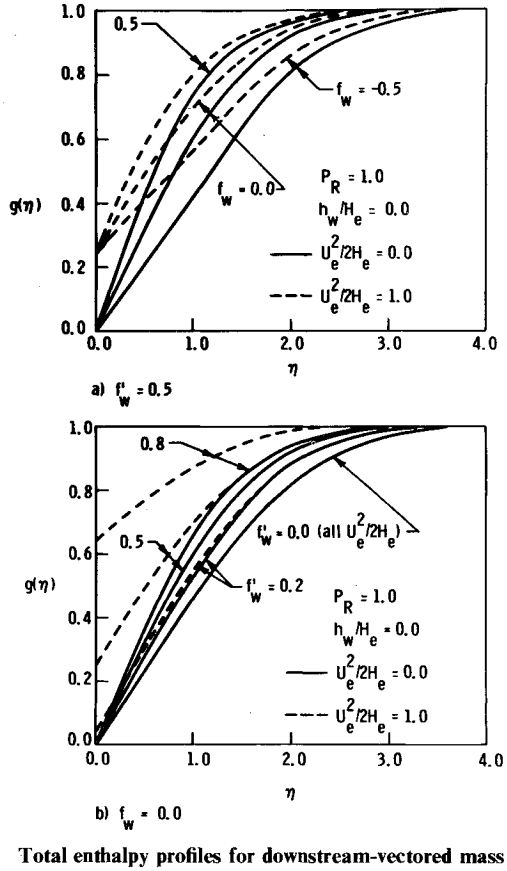

Fig. 6 Total enthalpy profiles for downstream-vectored mass transfer.

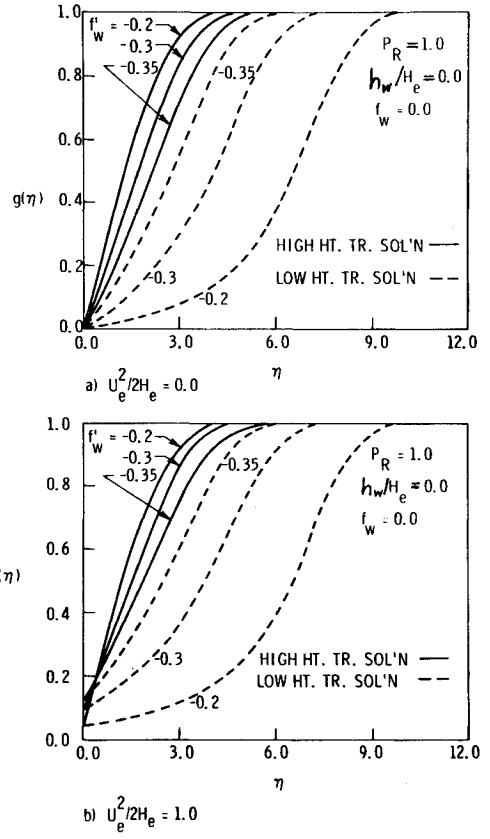

Fig. 7 Total enthalpy profiles for upstream-vectored mass transfer.

in terms of different nonsimilar upstream history effects (initial conditions) that occur in practice, as discussed in Ref. 11 and also by Libby and Liu.[12] In the presence of blowing $f_w < 0$, upstream vectoring tends to act like an adverse pressure gradient as regards the high shear solution behavior, whereas the opposite is true for suction, at least up to moderate upstream injection velocities.

Typical boundary-layer velocity profiles pertaining to downstream vectoring are shown in Fig. 4 for three different tangential velocities. As expected, normal injection increases the boundary-layer thickness whereas downstream tangential injection has the opposite effect. For supercritical vectored blowing ($f_w < -0.87574$, $f'_w > 0$), these profiles clearly exhibit the features of a mixing or free shear layer between coflowing streams. Some representative profiles with upstream injection are illustrated in Fig. 5. The high-shear branch solutions resemble ordinary attached-flow flat-plate boundary-layer profiles, whereas the low shear profiles more nearly correspond to the wake-like flow solutions computed by Kennedy.[13]

Enthalpy Field

Figures 6 and 7 illustrate the typical shape of the total enthalpy profiles on a cooled wall with downstream and upstream vectoring, respectively; the effects of f_w and f'_w are analogous to these shown above on the velocity profiles. These profiles also illustrate the effect of the viscous dissipation heating parameter $u_e^2/2H_e$. Figure 7 compares the total enthalpy profiles pertaining to the two solution branches obtained with upstream vectoring; the high shear branch solutions resemble ordinary enthalpy profiles whereas those for low shear resemble adiabatic wall enthalpy profiles because of the low value of heat transfer involved.

Figure 8 illustrates the influence of vectored suction and injection on the wall total enthalpy gradient g'_w for a cold wall and $Pr = 1$, as obtained from the following result of differentiating Eq. (9):

$$g'(0) \equiv g'_w = (1 - g_w)[f''_w/1 - f'_w] \tag{10}$$

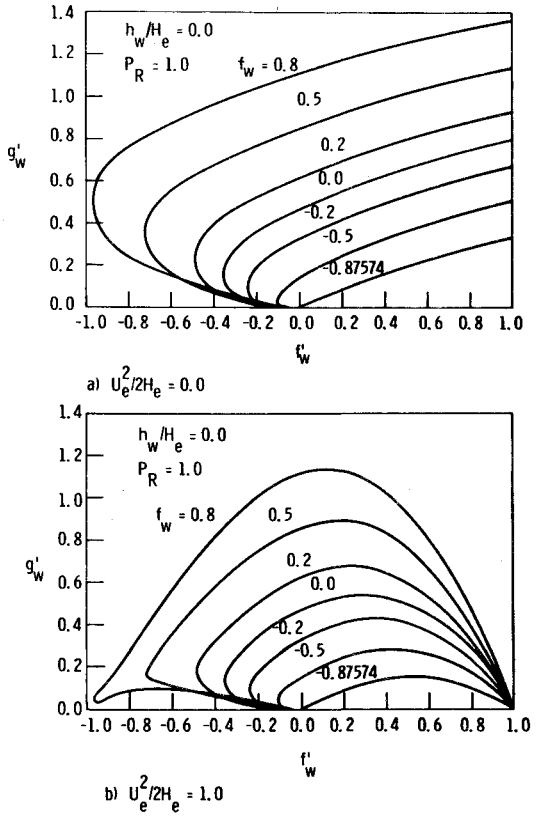

Fig. 8 Mass transfer vectoring effect on wall heat transfer parameter.

This represents the total heat transfer, since by Eq. 6 the explicit contribution of the frictional work associated with tangential injection vanishes for $Pr = 1$. Figure 8 shows the cold wall g'_w vs f'_w variation for $u_e^2/2H_e = 0$. For either upstream or small downstream vectoring, the enthalpy gradient follows the same trends as shown in Fig. 2 for the shear stress; in particular, it is seen that g'_w also possesses a double-branched solution character with upstream vectoring. However, for sufficiently strong downstream vectoring ($f'_w \gtrsim 0.2$), g'_w no longer follows the shear in decreasing with increasing f'_w but rather increases so as to approach a nonvanishing limiting value (which depends on f_w) as $f'_w \to 1$. This behavior can be understood by noting from Fig. 2 that f''_w vanishes like $(1-f'_w)$ as $f'_w \to 1$ with a constant of proportionality dependent on f_w; hence, from Eq. (10), g'_w must correspondingly approach a nonvanishing limit. Figure 8b shows the g'_w vs f'_w variation for $h_w/H_e = 0$ and $u_e^2/2H_e = 1$ (here, g_w is not constant along these curves but has the value f'^2_w). In this case the heat transfer more closely follows the shear variation of Fig. 2 and vanishes as $f'_w \to 1 (g_w \to 1)$. As was the case with the shear, we see that small amounts of downstream tangential injection cause an increase in the heat transfer followed by a subsequent decrease as f'_w is increased still further.

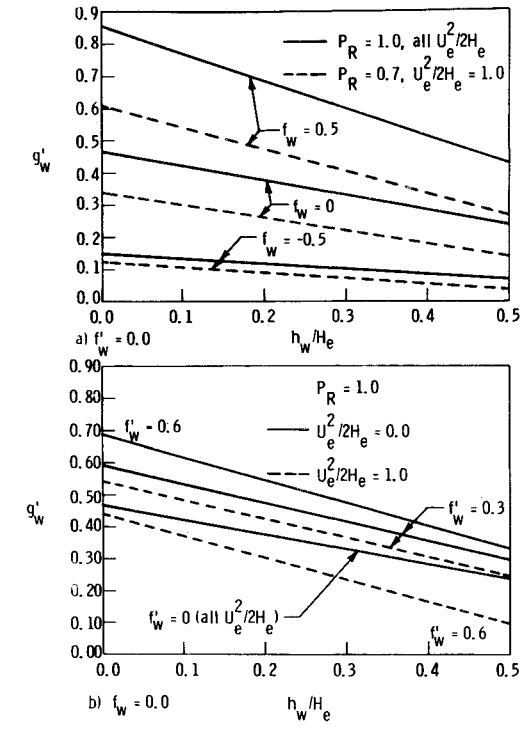

Fig. 9 Wall temperature and Prandtl number effects on wall heat transfer parameter.

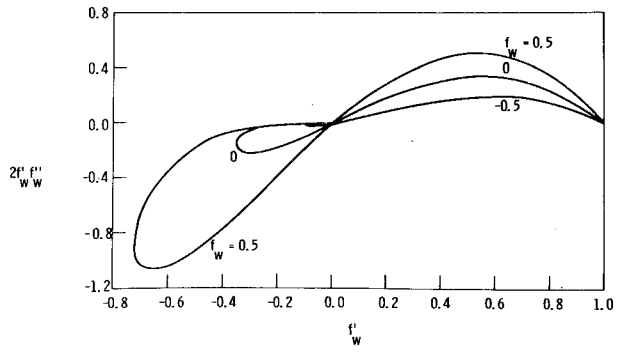

Fig. 10 Mass transfer vectoring effect on frictional work term.

The effect of nonunity Prandtl number due to viscous dissipation heating proportional to $u_e^2/2H_e$ is indicated in Fig. 9 for the case of high speed flow. When $Pr < 1$, the effect is generally to reduce g'_w, the magnitude of the reduction increasing with f_w; it is small for injection but becomes fairly large for suction owing to the enhanced size of the last term in Eq. (2). Also shown is the effect of wall temperature, which is essentially linear.

Figure 10 shows the frictional work term $2f'_w f''_w$ associated with vectored injection, which contributes to the surface heat transfer when $Pr \neq 1$ (see Eq. 6)§ as a function of both the normal and tangential mass transfer parameters. It is seen that small to moderate downstream injection velocities tend to increase this frictional work contribution; however, further increase in f'_w toward unity causes it to vanish since f''_w approaches zero. On the other hand, injection in the upstream direction changes the sign and increases the magnitude of the effect to rather large values depending upon the value of f_w. In both situations, these effects are increased as f_w is increased from negative to positive values.

Adiabatic Wall Recovery Temperature

For unity Prandtl number, Eqs. (6) and (9) show that for zero heat transfer, $g_w = H_w/H_e = 1$ and hence that

$$T_{a_w} = T_e + \frac{u_e^2 - u_w^2}{2C_p} = 1 + (1 - f'^2_w)\left(\frac{\gamma - 1}{2}\right) M_e^2 \qquad (11)$$

implying a recovery factor equal to $1-(f'_w)^2$. When $Pr \neq 1$, the energy Eq. (2), being a linear ordinary differential equation, can be integrated directly with the use of the integrating factor $\exp \int Prf\, d\eta$ to yield the following final result for an adiabatic wall:

$$\frac{T_{a_w}}{T_e} = 1 + (1 - f'^2_w - Z)\left(\frac{\gamma - 1}{2}\right) M_e^2 \qquad (12a)$$

§ Note that this term accounts for the entire wall heat transfer for wall temperatures such that $g'_w = 0$ when $Pr \neq 1$.

Table 2 Similar solutions for $Pr = 1.0$, all $u_e^2/2H_e$

f_w	f'_w	f''_w	$I_o/(g_w - f'_w)$	f_w	f'_w	f''_w	$I_o/(g_w - f'_w)$
	a) Downstream vectoring				−0.60	1.4123	0.8839
0.8	0.0	1.1100	0.7020		−0.80	1.3837	1.013
	0.2	0.9353	0.6660		−0.955	1.2201	1.240
	0.4	0.7342	0.6355	0.5	−0.20	0.9368	0.9165
	0.6	0.5098	0.6098		−0.40	0.9620	1.029
	0.8	0.2644	0.5875		−0.50	0.9441	1.113
0.5	0.0	0.8579	0.8398		−0.60	0.8908	1.239
	0.2	0.7402	0.7830		−0.72	0.6252	1.767
	0.4	0.5914	0.7370	0.20	−0.10	0.6323	1.100
	0.6	0.4165	0.6998		−0.20	0.6299	1.184
	0.8	0.2185	0.6685		−0.30	0.6056	1.301
0.2	0.0	0.6190	1.035		−0.40	0.5440	1.494
	0.2	0.5568	0.9380		−0.48	0.4040	1.924
	0.4	0.4578	0.8670	0.00	−0.15	0.4490	1.393
	0.6	0.3292	0.8118		−0.20	0.4301	1.480
	0.8	0.1756	0.7676		−0.25	0.4015	1.597
0.0	0.0	0.4696	1.217		−0.30	0.3566	1.774
	0.2	0.4431	1.073		−0.35	0.2575	2.225
	0.4	0.3751	0.9748	−0.20	−0.05	0.3177	1.556
	0.6	0.2752	0.9020		−0.10	0.2985	1.666
	0.8	0.1490	0.8450		−0.15	0.2700	1.821
−0.2	0.0	0.3305	1.468		−0.20	0.2250	2.078
	0.2	0.3381	1.242		−0.236	0.1578	2.551
	0.4	0.2985	1.104	−0.50	−0.02	0.1376	2.200
	0.6	0.2251	1.007		−0.04	0.1202	2.340
	0.8	0.1242	0.9340		−0.06	0.1098	2.507
−0.5	0.0	0.1484	2.112		−0.08	0.0903	2.754
	0.2	0.2012	1.588		−0.10	0.0589	3.292
	0.4	0.1977	1.348				
	0.6	0.1584	1.198				
	0.8	0.0910	1.091	Low shear solutions			
−0.8	0.0	0.0174	4.165	0.8	−0.20	0.0398	13.34
	0.2	0.0965	2.111		−0.40	0.1099	6.876
	0.4	0.1170	1.673		−0.60	0.2324	4.344
	0.6	0.1034	1.437		−0.80	0.4380	2.880
	0.8	0.0631	1.281		−0.955	0.7391	1.972
−0.87574	0.0	0.0	16.072	0.5	−0.20	0.0215	10.08
	0.2	0.0763	2.284		−0.40	0.0988	5.239
	0.4	0.1002	1.771		−0.50	0.1681	4.014
	0.6	0.0916	1.505		−0.60	0.2731	3.072
	0.8	0.0569	1.335		−0.72	0.6009	1.823
−0.90	0.05	0.0222	3.690	0.2	−0.10	0.0020	13.55
	0.2	0.0703	2.343		−0.20	0.0182	7.709
	0.4	0.0952	1.803		−0.30	0.0564	5.207
	0.6	0.0880	1.529		−0.40	0.1322	3.623
	0.8	0.0550	1.353		−0.48	0.2837	2.424
−1.0	0.05	0.0071	4.738	0.0	−0.15	0.0086	8.045
	0.20	0.0489	2.611		−0.20	0.0221	6.198
	0.40	0.0759	1.945		−0.25	0.0453	4.899
	0.60	0.0740	1.627		−0.30	0.0848	3.855
	0.80	0.0476	1.278		−0.35	0.1785	2.735
−1.25	0.05	0.0000	9.146	−0.20	−0.05	$6.77(10^{-5})$	15.69
	0.20	0.0151	3.458		−0.10	0.0028	8.889
	0.40	0.0393	2.356		−0.15	0.0138	6.191
	0.60	0.0454	1.902		−0.20	0.0410	4.466
	0.80	0.0320	1.635		−0.236	0.0952	3.239
				−0.50	−0.02	$2.65(10^{-7})$	20.73
	b) Upstream vectoring				−0.04	$1.68(10^{-4})$	11.40
High shear solutions					−0.06	0.0017	8.083
0.8	−0.20	1.2535	0.7465		−0.08	0.0069	6.133
	−0.40	1.3586	0.8040		−0.10	0.0237	4.467

where

$$Z = (1-Pr)\int_0^\infty \left[\int_0^\eta \frac{(f'^2)''}{(f'')^{Pr}}d\eta + 2f'_w(f''_w)^{1-Pr}\right](f'')^{Pr}\,d\eta \quad (12b)$$

As is well known, there is no effect of normal mass transfer on the recovery factory when $Pr = 1$; however, we see there is a reduction associated with tangential injection which in high-speed flows can be quite significant, as illustrated by the plot of Eq. (11) given in Fig. 11.

Momentum and Displacement Thicknesses

The influence of vectored mass transfer on the displacement thickness integral I_0 was also evaluated; typical results for the case $Pr = 1$ along with those for the wall shear parameter are given in Table 2. In this case, the two other integral thicknesses of interest, I_1 and I_2, can be calculated directly from the table by simple algebraic relationships as follows. By direct addition of the defining relationships for I_0 and I_2, the displacement

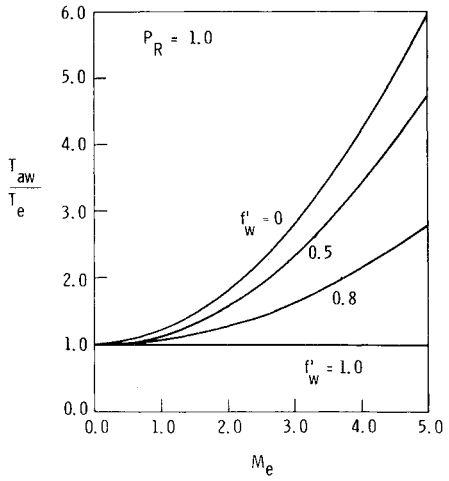

Fig. 11 Tangential injection effect on adiabatic wall temperature.

thickness integral I_1 is found to be

$$I_1 = I_0 + I_2 \tag{13}$$

whereas integration of Eq. (1) across the boundary layer and use of the result in the definition of I_2 yields

$$I_2 = f''_w - (1 - f'_w) f_w \tag{14}$$

Furthermore, the heat transfer parameter g'_w can be calculated from Table 2 by means of Eq. (10), noting that the result is linear in $1 - g_w$. Further illustrated detailed discussion can be found in Ref. 9.

IV. Conclusions

It is felt that the results of the present theoretical investigation provide useful insight into the influence of combined normal and tangential surface mass transfer on laminar boundary-layer skin friction, heat transfer, and thickness growth. The results also provide a basis for approximate engineering analysis of the problem by the local similarity method or by serving as profile models in moment methods (e.g., by Lees and his collaborators[6]). Moreover, with proper interpretation the present work should find practical application in a variety of boundary-layer mass transfer problems, such as the design of film and transpiration-cooling devices using distributed vectored injection, studies of vectored suction boundary-layer control on wings and engine inlets on high speed aerodynamic vehicles where the flow tends to be laminar, the use of upstream and downstream gas injection to produce aerodynamic control forces on hypervelocity bodies, investigations of the flow adjacent to moving mass transfer surfaces or per permeable walls with injection gas turning,[14] and in the study of the mixing of nonparallel gas streams as for example occurs in the flowfield around the massively ablating planetary entry probes anticipated for distant planets.[15]

There are several aspects of the present investigation which warrant further improvement to increase its practical utility. First, consideration of axial pressure gradient effects. Such a study for the case of viscous-inviscid interaction-induced pressure gradients important in hypersonic aerodynamics applications has in fact recently been completed by the authors.[16] Second, elimination of the local similarity assumption would enable the study of various streamwise distributions of vectored suction and film-injection such as the highly nonsimilar case of uniform mass transfer. An integral method approach would appear useful here. Third, in many practical problems a non-homogeneous flow with variable $\rho\mu$ and diffusion effects must additionally be taken into account due to injection of a liquid or gas differing significantly from that of the external flow. Fourth, there is the obvious practical need to treat the case of vectored injection into turbulent flow; the primary difficulty here of course is the lack of an eddy viscosity model valid over a wide range of mass transfer rates and angles.

References

[1] Scala, S. and Sutton, G., "Vectored Injection into a Hypersonic Laminar Boundary Layer," *Jet Propulsion*, Vol. 27, 1957, pp. 895–896.

[2] Wazzan, A. R., Lind, R. C., and Liu, C. Y., "Laminar Boundary Layer with Mass Transfer and Slip," *Physics of Fluids*, Vol. 11, June 1968, pp. 1271–1277.

[3] Fox, V. G., Erickson, L. E., and Fan, L. T., "Methods for Solving the Boundary Equations for Moving Continuous Flat Surfaces with Suction and Injection," *AIChE Journal*, Vol. 14, 1968, pp. 726–736.

[4] Sparrow, E. M. and Eckert, E. R. G., "Sensitivity of Skin Friction and Drag to the Distributions of Suction or Blowing," *Journal of the Aeronautical Sciences*, Vol. 29, Jan. 1962, pp. 104–105.

[5] Marvin, J. G. and Sinclair, A. R., "Convective Heating in Regions of Large Favorable Pressure Gradient," *AIAA Journal*, Vol. 5, Nov. 1967, pp. 1940–48.

[6] Reeves, B. L. and Lees, L., "Supersonic Separated and Reattaching Flows. Pt I," *AIAA Journal*, Vol. 2, Nov. 1964, pp. 1907–1920.

[7] Inger, G. R., "Vectored Injection into Isobaric Laminar Boundary Layer Flows," *"Wärme—und Stossübertragung,"* Vol. 5, 1972, pp. 201–203.

[8] Dewey, C. F. and Gross, J. F., "Exact Similar Solutions of the Laminar Boundary-Layer Equations," Rand Corporation Research Memorandum RM-5089-ARPA, July 1967, Rand Corporation, Santa Monica, Calif.

[9] Inger, G. R. and Swean, T. F., Jr., "Vectored Injection into Non-Adiabatic Boundary Layer Flows Including Incipient Separation," Department of Aerospace Engineering Report VPI-Aero-003, June 1973, Virginia Polytechnic Institute and State University, Blacksburg, Va.

[10] Emmons, H. W. and Leigh, D. C., "Tabulation of the Blasius Function with Blowing and Suction," Harvard University Combustion Aerodynamics Laboratory Rept. 9, 1953, Harvard University, Cambridge, Mass.

[11] Cohen, C. B. and Reshotko, E., "Similar Solutions for the Compressible Laminar Boundary Layer with Heat Transfer and Pressure Gradient," Rept. 1293, 1956, NACA.

[12] Libby, P. A. and Liu, T. M., "Further Solutions of the Faulkner Skan Equation," *AIAA Journal*, Vol. 5, May 1967, pp. 1040–1042.

[13] Kennedy, E. D., "Wake-Like Solutions of the Laminar Boundary Layer Equations," *AIAA Journal*, Vol. 2, Feb. 1964, pp. 225–231.

[14] Beavers, G. S. and Joseph, D. D., "Boundary Conditions at a Naturally Permeable Wall," *Journal of Fluid Mechanics*, Vol. 30, Pt. 1, 1967, pp. 197–207.

[15] Inger, G. R., "Viscous Effects in Massively-Ablating Planetary Entry Body Flowfields," *Journal of Spacecraft and Rockets*, Vol. 11, July 1974, pp. 540–541.

[16] Inger, G. R. and Swean, T. F., Jr., "Hypersonic Viscous-Inviscid Interaction with Vectored Surface Mass Transfer," VPI & SU Rept. Aero-012, March 1974, Virginia Polytechnic Institute and State University, Blacksburg, Va.